Compact x-ray microtomography system for element mapping and absorption imaging

J. M. Feldkamp,[a] C. G. Schroer, and J. Patommel
Institut für Strukturphysik, University of Technology Dresden, D-01062 Dresden, Germany

B. Lengeler, T. F. Günzler, and M. Schweitzer
II. Physikalisches Institut, RWTH Aachen University, D-52056 Aachen, Germany

C. Stenzel
Astrium-Space Transportation, Department: TO 611, Claude-Dornier-Strasse, D-88039 Friedrichshafen, Germany

M. Dieckmann
European Space Research and Technology Centre, Keplerlaan 1, Postbus 299, NL-2200 AG Noordwijk, The Netherlands

W. H. Schroeder
Phytosphere Institute, ICGIII, Research Center Jülich, D-52425 Jülich, Germany

(Received 13 March 2007; accepted 28 May 2007; published online 2 July 2007)

We have designed and built a compact x-ray microtomography system to perform element mapping and absorption imaging by exploiting scanning fluorescence tomography and full-field transmission microtomography, respectively. It is based on a low power microfocus tube and is potentially appropriate for x-ray diagnostics in space. Full-field transmission tomography yields the three-dimensional inner structure of an object. Fluorescence microtomography provides the element distribution on a virtual section through the sample. Both techniques can be combined for appropriate samples. Microradiography as well as fluorescence mapping are also possible. For fluorescence microtomography a small and intensive microbeam is required. It is generated using a polycapillary optic. Operating the microfocus tube with a molybdenum target at 12 W, a microbeam with a full width at half maximum lateral extension of 16 μm and a flux of about 10^8 photons/s is generated. As an example of application, this beam is used to determine the element distribution inside dried plant samples. For full-field scanning tomography, the x-ray optic is removed and the sample is imaged in magnifying projection onto a two-dimensional position sensitive detector. Depending on the sample size, a spatial resolution down to about 10 μm is possible in this mode. The method is demonstrated by three-dimensional imaging of a rat humerus. © *2007 American Institute of Physics.* [DOI: 10.1063/1.2751094]

I. INTRODUCTION

One of the key strengths of hard x-ray microscopy is the large penetration depth of hard x rays in matter, allowing one to investigate the inner structure of a sample without destructive sample preparation. In combination with tomography, these microscopy techniques make it possible to reconstruct the three-dimensional inner structure of an object. In full-field microscopy, the sample is imaged in transmission, recording full microradiographs of the object with a position sensitive detector. In this mode, attenuation and phase contrast can be exploited.[1–10]

Alternatively, in scanning microscopy, the sample is scanned with a small but intensive microbeam. The main advantage here is that a variety of x-ray analytical techniques can generate contrast, such as x-ray fluorescence, absorption spectroscopy, and diffraction, yielding local elemental, chemical, and nanostructural information, respectively. When combined with tomography, this information can also be obtained from inside the sample.[11–14] Due to the sequential data acquisition, however, scanning microscopy is much slower than the full-field techniques. Compared to scanning electron microscopy, x-ray techniques have the advantage that no bremsstrahlung is generated by the x-ray probe, yielding a high detection sensitivity for element analysis by fluorescence photons.

In the last few years, the development of all these techniques has greatly benefited from the advent of third generation synchrotron radiation sources and significant improvements in x-ray optics. The high brilliance[15] of synchrotron radiation sources is crucial in pushing these techniques to the limit. However, the availability of synchrotron radiation is very limited, and x-ray microscopy in the laboratory, the field, or in space is highly desirable. One promising approach here is to use an x-ray microfocus source, since it combines a small source size and low power consumption with a (relatively) high brilliance compared to other laboratory sources.

X-ray microscopy and microtomography with x-ray

[a]Electronic mail: feldkamp@physik.tu-dresden.de

 © 2007 American Institute of Physics

Downloaded 02 Jul 2007 to 141.30.244.6. Redistribution subject to AIP license or copyright, see http://rsi.aip.org/rsi/copyright.jsp

FIG. 1. (Color online) X-ray microtomography system for element mapping and absorption imaging.

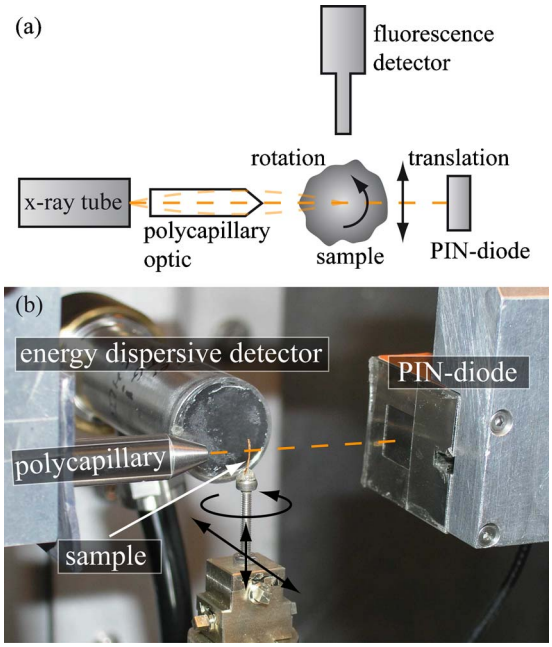

FIG. 2. (Color online) (a) Schematic sketch in top view and (b) closeup photograph in side view of the experimental setup for fluorescence mapping and tomography. The polycapillary optic focuses the x rays from the microfocus tube onto the sample, which is mounted on a goniometer head. The transmitted signal and the fluorescence radiation are recorded with a PIN diode and a fluorescence detector, respectively.

tubes have been widely investigated using full-field imaging (especially on bones as reference samples[16–19]) as well as scanning fluorescence techniques.[3,20] Commercially available systems have been built for both modes.[21,22]

The aim of this project—supported by the European Space Agency (ESA)—was to identify x-ray microscopy techniques that can be implemented in a stand-alone compact device based on a low power microfocus x-ray tube, potentially appropriate for x-ray diagnostics in microgravity. A scanning and a full-field technique were selected for implementation in this device, i.e., x-ray fluorescence tomography and cone-beam projection tomography. Both techniques were implemented in a compact "technology demonstrator," designed, constructed, and tested within the project. One important feature of this device is that both techniques can be combined and sequentially performed on the same sample without manual intervention.

In this article, this device is described and the results from a variety of reference experiments are given to demonstrate its performance. In Sec. II, we discuss the strategy to implement x-ray scanning microscopy with a microfocus x-ray tube and describe the resulting scheme for the implementation of both microscopy techniques. Section III describes the reference experiments, i.e., scanning fluorescence tomography and microscopic mapping of freeze dried plant samples (Sec. III A) and full-field tomography of a bone sample and microradiography of an electronic circuit (Sec. III B). A detailed description of the setup is given in the appendix.

II. DESIGN AND IMPLEMENTATION

An important property of an x-ray source is its brilliance, which is defined as the number of monochromatic (0.1% bandwidth) photons emitted per second into a certain solid angle for a given source size. Compared to a typical synchrotron radiation source, the brilliance of an x-ray tube is about ten orders of magnitude lower. For scanning fluorescence microscopy with a laboratory source, this means that the experimental requirements have to be scaled down substantially. Any focusing optic is required to capture as large a solid angle as possible and thus bring as many photons as possible into the x-ray focus. The demands for the focal size have to be relaxed also, such as to allow a higher photon flux at a larger spot size. As an optic, we selected a polycapillary optic, which images the x-ray source point to point onto a secondary focus exploiting total external reflection. Other focusing devices, such as a doubly bent crystal and doubly curved multilayer optics, were tested and characterized in the development phase. However, the polycapillary was favored for this application, because—compared to the other optics in question—it has a superior performance with respect to focal flux and beam size and is also less demanding in handling and alignment.

In the following, we present the general design of the scanning and full-field microtomography system and give an overview of the main components. We consider the specifics of the two modes of operation in more detail.

A. General layout

The instrument described here is a stand-alone unit mounted on a laboratory trolley as shown in Fig. 1. The trolley measures 1250×800 mm^2; the total height of the device is 1510 mm. The dimensions of the experimental chamber itself are $620 \times 540 \times 610$ mm^3.

Two experimental techniques, scanning fluorescence microtomography and magnifying full-field absorption tomography, are implemented. Switching between the two experimental modes is automated, so that no manual intervention is required. In principle, this allows one to sequentially apply both modes of operation to the same sample and thus determine the (three-dimensional) structure of an object and link it to the distribution of chemical elements inside it. The

Downloaded 02 Jul 2007 to 141.30.244.6. Redistribution subject to AIP license or copyright, see http://rsi.aip.org/rsi/copyright.jsp

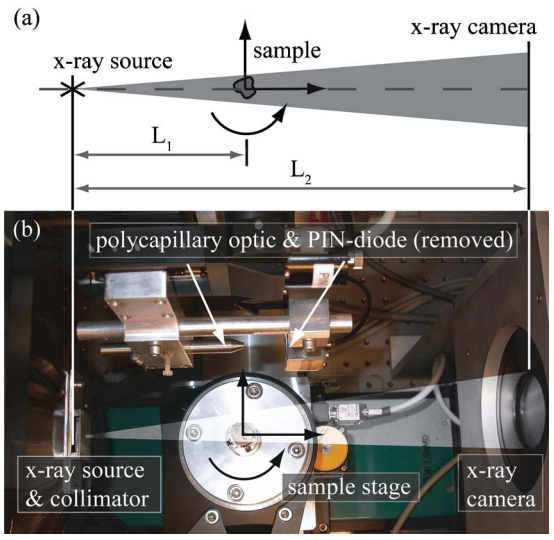

FIG. 3. (Color online) (a) Schematic sketch and (b) photograph of the experimental setup for transmission radiography and tomography (both in top view). The focusing optic and the PIN diode are moved out of the beam, exposing the two-dimensional x-ray camera mounted at a fixed distance from the source.

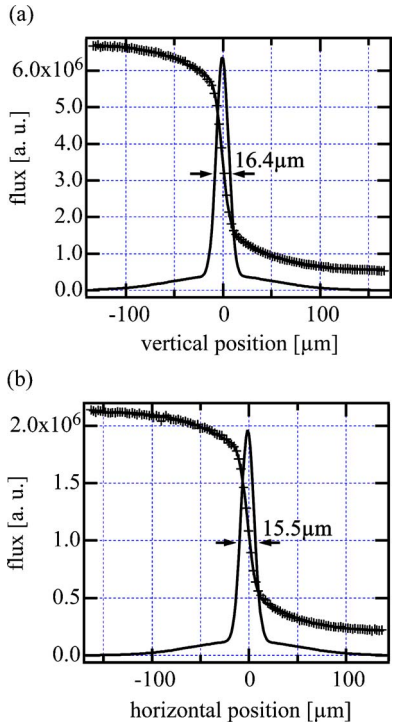

FIG. 4. (Color online) (a) Vertical and (b) horizontal knife edge scans through the focus of the polycapillary optic.

sample for such an experiment has to be transparent enough to its fluorescence light, yet have a high enough contrast in projection tomography.

The major components of the microtomograph (see Figs. 2 and 3 for pictures of the sample environment) are a microfocus x-ray tube, a focusing polycapillary optic, a sample stage for tomographic scanning, a fluorescence detector, a PIN diode, and a two-dimensional position sensitive detector, all placed inside a radiation protection box, so that no additional shielding is required for safe operation. All control and evaluation electronics are included in this compact setup. Supplies for power and the cooling water needed for the fluorescence detector are provided externally. Detailed descriptions and technical specifications of the major components may be found in the appendix.

B. Scanning fluorescence analysis

For fluorescence scanning microscopy—whether studying the element distribution of a sample by scanning two translations or recording a tomogram—a small x-ray focus is needed. In our setup, x rays from a microfocus x-ray tube are focused onto the sample using a polycapillary optic [see Fig. 2(a) for a schematic sketch of the experimental setup]. The sample stage allows for automated sample motion in three translational and one rotational degrees of freedom about the vertical axis. The sample is centered about the rotation axis of the stage using a manually adjustable goniometer head. The fluorescence detector is positioned close to the sample, as shown in Fig. 2(b). The sample-to-detector distance is variable in order to adjust the solid angle determined by the active area of the detector, thus adjusting the flux of fluorescence photons in the detector. The other degrees of freedom of this detector are prealigned and fixed. A PIN diode is positioned a few millimeters behind the sample to measure the transmitted radiation.

To set up a fluorescence experiment, the optic and the PIN diode are moved into the beam and adjusted using three translations. The polycapillary must first be aligned to bring the x-ray source point into the primary focus of the optic. This is done by optimizing the flux transmitted by the polycapillary. For a molybdenum target, a flux of 1.4×10^8 photons/s is measured in the focus.[23] The PIN diode is fixed with respect to the optic, prealigned with the opical axis of the latter.

The alignment of the polycapillary optic can be done automatically by scanning the optic through the beam and maximizing the current in the PIN diode. Manual alignment is not required. After this, the sample can be moved into the secondary focus of the optic, which is approximately 4 mm behind the exit of the polycapillary. The exact position of the focus is found by scanning a knife edge as a sample. For Mo $K\alpha$ radiation, the spot size at the focus was measured to be around 16 μm both horizontally and vertically. A knife edge scan of the focus is displayed in Fig. 4.

In two-dimensional translational mapping, the horizontal and vertical translations are both scanned perpendicularly to the optical axis to generate a two-dimensional element map. This is useful for objects that are mainly two dimensional, e.g., leaves from plants. In this case, tomographic imaging is not required to interpret the element distribution inside the sample.

To obtain a fluorescence tomogram, each projection is recorded by scanning the sample horizontally through the microbeam in N steps and recording the fluorescence and transmitted radiation at each position in the scan with the fluorescence detector and the PIN diode, respectively. At the first and the last scan positions the sample is not illuminated by the microbeam, recording two blank points, which are

Downloaded 02 Jul 2007 to 141.30.244.6. Redistribution subject to AIP license or copyright, see http://rsi.aip.org/rsi/copyright.jsp

TABLE I. Engineering specifications of the microtomography system.

X-ray source—microfocus x-ray tube	
Acceleration voltage	10–100 keV
Target material	Cu, Mo, Ag (exchangeable)
Source size	<3 μm at 3 W additional 0.7 μm per watt for power >3 W
Maximum power	40 W
X-ray microfocus properties[a]	
Spot size	16×16 μm^2
Depth of focus	225 μm
Flux	1.4×10^8 photons/s at 12 W
Fluorescence detector	
Energy range	$\approx$1–30 keV
Energy resolution	144 eV at Mn $K\alpha$
X-ray camera	
Array size	1250×1152
Pixel size	22.5×22.5 μm^2
Field of view	28.1×25.9 mm^2

[a]X-ray microfocus properties obtained using a Mo target and an acceleration voltage of $U=60$ kV

used to measure the primary flux needed for normalization. After a scan is completed, the sample is rotated by an integer fraction of 360° and the translational scan is repeated. This procedure is iterated until the sample has completed one full rotation.

According to Nyquist's theorem the translational scanning step size should be half the size of the microbeam in order to obtain ideal sampling. With a 16 μm x-ray focus, the highest spatial resolution is therefore obtained for a scanning step size of about 8 μm. If the sample is too large, however, it may become necessary to trade in spatial resolution for a shorter acquisition time for the full scan. For scanning tomography, the acquisition time grows quickly with the number N of positions in one translational scan, since the number of rotations M should be roughly $M\approx\pi N/2$ in order to maintain the spatial resolution defined by the number of scanning steps.[24] The overall acquisition time T of the tomogram is therefore given by $T=NMt\approx N^2(\pi/2)t$, where t is the acquisition time at each position of the scan. For this reason, careful prealignment of the sample is crucial to minimize the acquisition time, as any sample misalignment will increase the required scanning steps, increasing the overall acquisition time quadratically. To acquire a fluorescence tomogram of highest spatial resolution, the sample's diameter, in any case, must not exceed the depth of the x-ray focus of 225 μm (see Table I).

The fluorescent light excited inside the sample may be significantly attenuated by the sample itself on its way to the detector. The attenuation inside the sample for a specific fluorescence energy is not known *a priori* and is not directly accessible in the experiment (as opposed to the overall attenuation for the incoming x rays, which is measured by the PIN diode). Therefore, during the tomographic reconstruction, the attenuation is iteratively estimated for all fluorescence lines, starting with the most energetic.[25]

C. Full-field transmission radiography and tomography

For transmission radiography and tomography, the optic and the PIN diode are removed from the beam path, exposing the x-ray camera located at a fixed distance $L_2=270$ mm away from the source, as shown in Fig. 3. The source-to-sample distance L_1 can be varied from 23 to 176 mm, allowing one to choose the magnification $(m=L_2/L_1)$ continuously between 1.5× and 11.9×.

To acquire a full-field tomogram, a number M of projection images is recorded at evenly spaced angular positions over a full rotation. M is chosen such as to approximately fulfill the angular sampling condition $M\approx\pi N/2$, where N is the maximum number of pixels spanned by the sample. Additionally, flat-field images and dark-field images are acquired to be able to normalize the projection images and correct them for detector dark current and readout noise.

The achievable magnification for tomography is limited by the sample size because the object must fit into the cone defined by the source and the detector area (opening angle $\approx12°$). The largest possible sample size in this setup is about 17 mm in diameter at the lowest magnification. Larger magnification factors are achievable (only) with smaller samples. The transmission tomography setup is displayed in Fig. 3(b).

The reconstructions of tomograms in this cone-beam geometry are done with commercial software (COBRA by Exxim Computing Corporation, Pleasanton, CA, USA), exploiting the Feldkamp algorithm.[26]

D. Safety and space accommodation

A basic investigation on safety aspects and a first analysis concerning the accommodation of an x-ray facility into a standard rack on the International Space Station (ISS) was performed in addition to the technical development of the system. In this conceptual layout, 83% of the available rack space is used and 200 kg of the total allowable payload mass is still available.

Besides standard safety issues such as structural integrity and fire and electrical safety, the use of x rays and the mandatory high voltage for their generation have been identified as particular safety issues for an x-ray diagnostics facility.

For the ISS, no special regulations for the use of x rays are determined. Instead, the individual operator's national regulations for radiation protection have to be met. Appropriate shielding of the x-ray source and the experimental chamber against radiation, as well as an interlock system for the operation of the x-ray tube, have to be provided. Both of these topics can be addressed by a proper design of the flight facility and by dedicated verification procedures. However, the shielding puts an additional burden on the mass budget.

Concerning the application of high voltage, safety regulations require a three-failure tolerance which has to be fulfilled for all operational conditions. To cope with this requirement and to keep the necessary design impacts limited as well it would be required in a future ISS device to keep the high voltage cables as short as possible and to avoid any

Downloaded 02 Jul 2007 to 141.30.244.6. Redistribution subject to AIP license or copyright, see http://rsi.aip.org/rsi/copyright.jsp

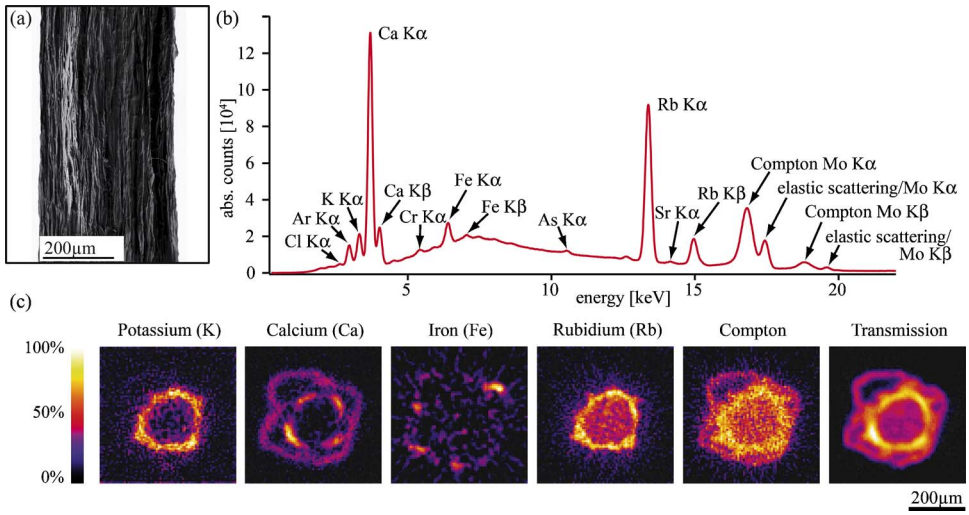

FIG. 5. (Color online) (a) Scanning electron microscope (SEM) image of a root of *Chamaecyparis* (yellow false cypress). (b) Accumulated spectrum obtained by summing up the individual spectra of all points of a fluorescence tomographic scan. In this way even elements with fairly low concentrations could be identified. The detected elements range from chlorine to strontium. (c) Reconstructed element maps on a virtual slice through the sample recorded by fluorescence microtomography. All pictures are color scaled individually. Only the stronger signals of the K $K\alpha$, Ca $K\alpha$, Fe $K\alpha$, and Rb $K\alpha$ [cf. spectrum in (b)] could be used for reconstruction with a reasonable signal-to-noise ratio. The signals of the Compton scattering peak and the transmission signal from the PIN diode were also reconstructed.

high voltage plug. As a consequence, the high voltage generator would have to be directly attached to the x-ray tube without any interface which can be disconnected.

Besides those mentioned above, further issues have been identified as critical to safety. Beryllium is used as a target substrate in the x-ray tube as well as for radiation windows in all of the detectors. This poses a safety threat, as toxic beryllium dust may be released and endanger the crew and potentially the whole mission, if a beryllium window accidentally breaks during operation. For this reason, the use of beryllium is categorically ruled out by space agencies and, accordingly, any parts concerned would have to be replaced by alternative materials, such as aluminium or kapton.

Furthermore, the high voltage generator uses oil as insulation fluid, which firstly reveals the danger of leakage and secondly the hazard of a loss of proper insulation, due to the different behavior of fluids under weightlessness. A solution may be a generator with a solid insulation.

III. REFERENCE EXPERIMENTS

A. Element specific fluorescence experiments

1. Scanning fluorescence microtomography

In view of possible plant physiological studies in space, we have applied fluorescence tomography to dried plant samples. Since elaborate specimen preparation may not be available in space station applications the simplest possible preparation protocol was applied as one test application. As an example, a dried root of *Chamaecyparis* (yellow false cypress) from the montane fog forests of Taiwan was inves-

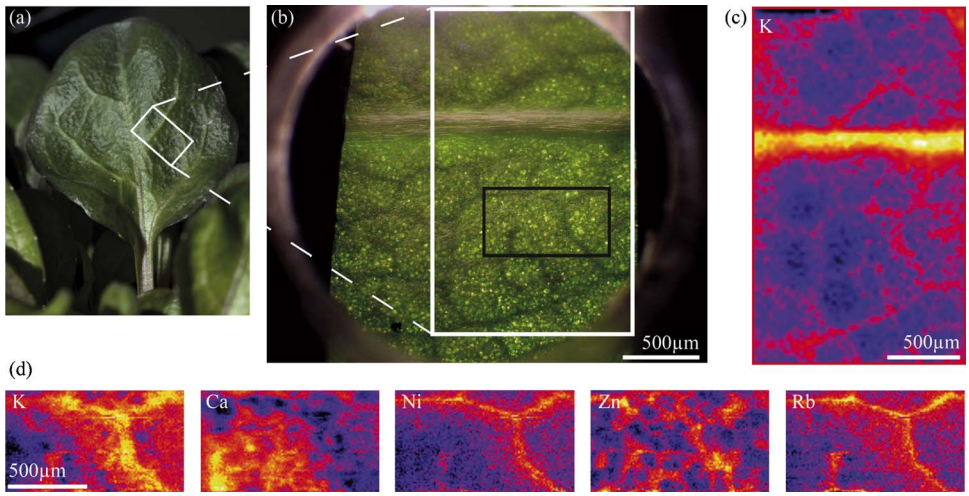

FIG. 6. (Color online) Two-dimensional fluorescence element mapping of a leaf of *Thlaspi caerulescens*. A section of the leaf shown in (a) was shock frozen in melting propane and freeze dried at −100 °C in ultrahigh vacuum. The freeze dried sample mounted in the sample holder (b) was scanned with the microbeam in two two-dimensional scans over the regions marked by the white and black rectangles depicted in (a) and (b). (c) The potassium (K) distribution in the coarsely scanned larger region (white rectangle) already reveals some features such as the major and some minor veins in the leaf. (d) Distributions of potassium (K), calcium (Ca), nickel (Ni), zinc (Zn), and rubidium (Rb) in the small region (black rectangle), scanned at maximum resolution.

Downloaded 02 Jul 2007 to 141.30.244.6. Redistribution subject to AIP license or copyright, see http://rsi.aip.org/rsi/copyright.jsp

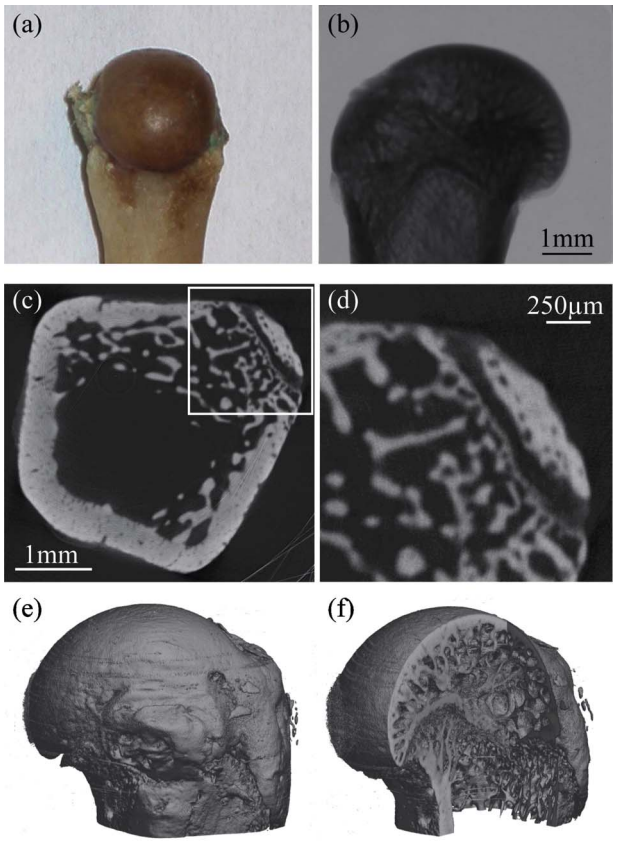

FIG. 7. (a) (Color online) Photograph of the ball joint of a rat humerus (sample provided by Felsenberg Charity, Berlin, Germany). (b) X-ray microradiograph of the joint. [(c)–(f)] Cone-beam tomographic reconstructions of the ball joint from 720 projections. (c) Single slice. (d) Magnified image of the rectangular region shown in (c). The smallest features are about 10 μm in size. (e) Three-dimensional (3D) rendering of the ball joint. (f) Virtual sectioning of the 3D rendering, revealing the trabecular structure inside the bone.

tigated. *Chamaecyparis* trees are able to take up a useful fraction of their nutrient supply from the deposition of dense fog.[27] The investigated sample originates from a tracer study where leaves were artificially misted with Rb as tracer in order to quantify the uptake and transport of fog tracers into the roots of the plant.

The sample [see the SEM image in Fig. 5(a)] was scanned through a microbeam of 16 μm lateral size in 72 horizontal steps of 7 μm and 93 rotations. At each position in the scan a full spectrum was recorded in 30 s acquisition time. The concentrations of the elements of interest were extracted from the spectra by calculating the background subtracted peak integrals. The integrated spectrum over all scan points is displayed in Fig. 5(b).

A tomographic reconstruction was done individually for each fluorescence line that has a sufficient signal-to-noise ratio. Figure 5(c) shows the tomographic reconstructions of the element distributions of potassium, calcium, iron, and rubidium. Additionally, the Compton scattering and transmission signal, i.e., the attenuation of the illuminating radiation inside the sample, were reconstructed. Note that each image is color scaled to its individual maximum. These element distributions allow one to measure the uptake and transport of physiologically relevant ions in plants.

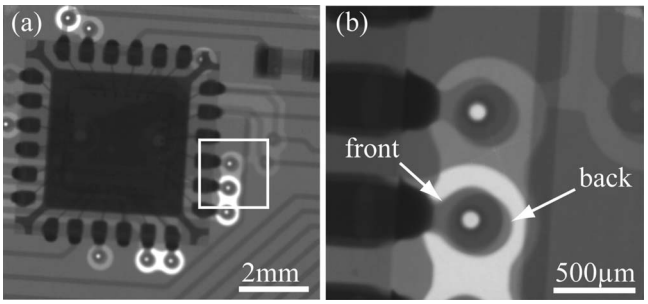

FIG. 8. (a) Microradiograph of a circuit board for the electronics of a silicon microstrip detector imaged with $m=3.5\times$ magnification. (b) Microradiograph of the rectangular region marked in (a) recorded at a magnification of $m=16\times$ ($L_1=17$ mm). The contacts on both sides of the board, pointed at by the arrows, are poorly aligned.

2. Two-dimensional (2D) mapping

The method of two-dimensional element mapping is demonstrated on a leaf of *Thlaspi caerulescens*, a heavy metal hyperaccumulator plant.[28] This leaf was loaded via the petiole by transpiration for three hours with a multielement cocktail of tracers. The tracers were rubidium, nickel, and zinc supplied as chlorides and nitrates at 5 mmol/L in Hoagland solution[29] at 1/10 dilution. These metals are of interest to the transport physiology of metals in plants and to studies involved in phytoremediation.

The sample and the results are presented in Fig. 6. We first scanned at medium resolution to identify regions of interest and then investigated a smaller field at maximum resolution. In Figs. 6(a) and 6(b), these two regions are marked by the white and black rectangles, respectively. The potassium distribution imaged by the large-field scan (white rectangle) is shown in Fig. 6(c). The high resolution element map was scanned over a field of 113 by 64 pixels, corresponding to the black rectangle in (b), at a step increment of 10 μm. The element distributions of potassium (K), calcium (Ca), rubidium (Rb), nickel (Ni), and zinc (Zn) are displayed in Fig. 6(d). K, Ni, and Rb remain in the veins, while the Ca and Zn concentrations are moved beyond this tissue.

B. Magnifying projection imaging

1. Tomography

With regard to space medicine, examining physiological parameters of small mammals under microgravity conditions promises to be very instructive. The goal of this experiment was to visualize and investigate the inner structures of a bone at high resolution without having to section it. Various studies have targeted this topic.[16–19] The interesting parameters include the density of the trabecular bone or the muscle-to-fat ratio, which are crucial values for osteoporosis or muscle decay studies in weightlessness. The sample we investigated in a reference experiment using magnifying projection tomography was a rat humerus [upper arm bone, see Fig. 7(a)].

One projection image of the bone is shown in Fig. 7(b). The magnification in this experiment was $m=4.1\times$ ($L_1=66$ mm). We recorded 720 projections with an exposure time of 20 s each. Including all images necessary for reconstruction, the acquired data set comprises 2 Gbytes and required an overall acquisition time of about 5 h, taking into

Downloaded 02 Jul 2007 to 141.30.244.6. Redistribution subject to AIP license or copyright, see http://rsi.aip.org/rsi/copyright.jsp

account dead times generated by detector readout and motor movement. The tomogram was reconstructed using the Feldkamp cone-beam reconstruction algorithm.[26] The overall processing time for this tomogram was approximately 2 h on the built-in computer [Intel P4, 2.0 GHz, 2 Gbytes random access memory (RAM)].

Reconstructions are shown in Figs. 7(c) and 7(d). The smallest features in these reconstructions are about 10 μm in size. Three-dimensional rendering images and virtual sections are displayed in Figs. 7(e) and 7(f). The trabecular bone is clearly resolved in this tomogram. This is, for example, important for long-term studies on bone evolution under weightlessness.

2. Radiography

To demonstrate magnifying radiography, a faulty printed circuit board (PCB) was imaged and investigated. Both its sides are part of the electric circuit. An accurate alignment of the two sides is therefore crucial for the functioning of the PCB. Two images, recorded at 3.5× and 16× magnifications, are depicted in Figs. 8(a) and 8(b), respectively.[30] The highly resolved image in Fig. 8(b) reveals that the front and the back of the circuit board are misaligned, which in this case was the reason for the failure.

IV. DISCUSSION

In this article, we have shown that state-of-the-art x-ray tomography in both fluorescence mode and magnifying projection mode are well feasible at high resolutions using a compact laboratory setup. Both techniques can be implemented in the same instrument and may be applied sequentially to the same sample, yielding new prospects of diagnosis. If additional safety requirements are addressed, a similar device could be brought to the International Space Station to enable x-ray diagnostics in weightlessness. From this a large spectrum of scientific fields would benefit, ranging from life science and space medicine to material science.

ACKNOWLEDGMENTS

The humerus bone was provided by D. Felsenberg. This project was funded by ESA/ESTEC under ESTEC/Contract No. 16327/02/NL/CK.

APPENDIX: COMPONENTS AND DEVICES

In the following, technical details of the components and devices incorporated in the system are described. The most important technical specifications of the major components are summarized in Table I.

1. X-ray source

The source is a Viscom XT9160-T microfocus x-ray tube, equipped with a molybdenum (Mo) transmission target (exchangeable for other materials) which can be operated at 10–100 kV with electron currents of 10–400 μA. This results in an operating power between 0.1 and 40 W. The vendor specification for the electron beam size is below 3 μm when operating at a power of less than 3 W. Above this value, the beam size increases by 0.7 μm for every additional watt of power. The temporal variations of the electron beam on the target are specified to be smaller than 2 μm.

For the imaging experiments, we chose a voltage of 60 kV and a current of 50 μA (3 W) in order to maintain a small spot size and optimize the sharpness in the images. For the fluorescence experiments, the power can be increased to match the spot size with the acceptance of the polycapillary. This allows operation at a current of 200 μA at the same voltage of 60 kV (12 W), yielding an increased photon flux in the x-ray focus. The transmission target used in this x-ray tube is a thin layer of molybdenum on a beryllium substrate, which also acts as the radiation window. The target can be removed manually for maintenance purposes and can be replaced by targets made from other materials, e.g., silver or copper.

2. Optic

The focusing x-ray optic is a monolithic polycapillary optic fabricated by X-Ray Optical Systems Inc. (XOS), East Greenbush, NY, USA. By scanning a gold knife edge through the focus, we measured a focal size of 16.4 μm [full width at half maximum (FWHM)] in vertical direction and 15.5 μm (FWHM) in horizontal direction (Fig. 4) at a flux of 3.6×10^7 photons/s for an x-ray tube power of 4 W. The depth of focus is 225 μm. The beam divergence was 65 mrad.

3. Fluorescence detector

To record the fluorescence radiation, an energy dispersive x-ray detector (EDX), model SuperDry II by Thermo Noran (Thermo Scientific, Waltham, MA, USA) is used. It is a Peltier-cooled lithium-doped silicon crystal [Si(Li)] detector. The warm end of the Peltier element is cooled by an external chiller unit, which maintains a constant temperature of 15 °C. The Si(Li) crystal has an active area of 10 mm^2 at a thickness of 3 mm. Its nominal energy resolution at Mn $K\alpha$ is 144 eV. The data is processed by a multichannel analyzer (MCA) with 2048 channels.

4. PIN diode and picoammeter

The transmitted radiation in the fluorescence experiments is recorded with a Hamamatsu PIN diode (model S3590-02 by Hamamatsu Photonics K.K., Hamamatsu City, Japan), enclosed by a custom-built housing with a Be window to guard it against visible light. It has an active area of 9×9 mm^2 and an effective thickness of 305±8 μm. The diode's output current is amplified by a picoammeter (Model 6485 Picoammeter, Keithley Instruments Inc., Cleveland, OH, USA). The PIN diode was characterized and calibrated with monochromatic synchrotron radiation.

Downloaded 02 Jul 2007 to 141.30.244.6. Redistribution subject to AIP license or copyright, see http://rsi.aip.org/rsi/copyright.jsp

5. X-ray camera

The two-dimensional x-ray camera used for transmission radiography and tomography is a charge-coupled device (CCD) based detector, model A-DY432, by Andor Technology, Belfast, Northern Ireland. The conversion of x rays to visible light is achieved using a $GdSO_4$ phosphor, which is then projected onto the CCD chip by a 1:1 fiber optic. The chip features 1250×1152 pixels of 22.5×22.5 μm^2 size each and allows readout rates of up to 0.6 frames/s. The CCD chip of the camera is operated at about -35 °C to reduce the dark current and readout noise. The chip is cooled by a Peltier element, which is in turn air cooled. The camera is protected by a beryllium window.

6. Motorization

The experimental chamber features two major groups of motors: the optic stage and the sample stage. The optic stage, mounted to the ceiling of the chamber, holds the polycapillary optic and the PIN diode needed for the fluorescence experiments. It has three translational degrees of freedom, which are necessary to align the optic in the beam. The translations are also used to remove the optic from the x-ray beam for full-field transmission radiography.

The sample stage is used to position and scan the sample in three translational and one rotational degrees of freedom. The translational motor along the optical axis is needed to focus the sample in fluorescence mode and to set the magnification in cone-beam geometry experiments (details in Secs. II B and II C, respectively).

All stage positioners are fabricated by MICOS (Eschbach, Germany). In addition to the stages described above, the fluorescence detector has a built-in motorized translation stage and can be retracted from the sample when it is not needed. A top view of the experimental chamber in transmission mode showing some of the motorization is displayed in Fig. 3.

7. Radiation protection

To be able to operate the microtomograph safely as a stand-alone device without any further infrastructure, full radiation protection around the x-ray tube and the experimental chamber is required. We constructed a protective housing from aluminium-lead-steel sandwich shielding plates. The thicknesses of the constituent plates are 1 mm for the steel and aluminium plates and 4 mm for the lead plates. Access to the chamber is granted by a sliding lead glass window. For user safety, an interlock system is installed.

Outside of the protection box, no radiation above normal level could be measured. The tomograph received clearance for independent operation from German radiation protection authorities.

8. Computation

A computer, including a screen and input devices, is accommodated in the trolley. The computer controls the x-ray tube as well as all motors and detectors via controlling software developed in-house. All necessary data analysis and tomography reconstruction softwares are also installed.

[1] J. C. Elliot and S. D. Dover, J. Microsc. **126**, 211 (1981).
[2] C. Raven, A. Snigirev, I. Snigireva, P. Spanne, S. Souvorov, and V. Kohn, Appl. Phys. Lett. **69**, 1826 (1996).
[3] A. Sasov and D. Van Dyck, J. Microsc. **191**, 151 (1998).
[4] P. Cloetens, W. Ludwig, J. Baruchel, D. Van Dyck, J. Van Landuyt, J. P. Guigay, and M. Schlenker, Appl. Phys. Lett. **75**, 2912 (1999).
[5] U. Bonse and F. Beckmann, J. Synchrotron Radiat. **8**, 1 (2001).
[6] Y. Wang *et al.*, Rev. Sci. Instrum. **72**, 2062 (2001).
[7] A. Sasov, Proc. SPIE **4503**, 274 (2002).
[8] C. G. Schroer *et al.*, Appl. Phys. Lett. **81**, 1527 (2002).
[9] C. G. Schroer, P. Cloetens, M. Rivers, A. Snigirev, A. Takeuchi, and W. Yun, MRS Bull. **29**, 157 (2004).
[10] F. Pfeiffer, T. Weitkamp, O. Bunk, and C. David, Nat. Phys. **2**, 258 (2006).
[11] A. S. Simionovici *et al.*, IEEE Trans. Nucl. Sci. **47**, 2736 (2000).
[12] C. G. Schroer *et al.*, Appl. Phys. Lett. **82**, 3360 (2003).
[13] B. Golosio, A. Somogyi, A. Simionovici, P. Bleuet, J. Susini, and L. Lamelle, Appl. Phys. Lett. **84**, 2199 (2004).
[14] C. G. Schroer, M. Kuhlmann, S. V. Roth, R. Gehrke, N. Stribeck, A. Almendarez-Camarillo, and B. Lengeler, Appl. Phys. Lett. **88**, 164102 (2006).
[15] The brilliance of an x-ray source is defined as the monochromatic (0.1% bandwith) flux per source area and solid angle.
[16] J. Waarsing *et al.*, Bone (N.Y.) **34**, 163 (2004).
[17] P. Rüegsegger, B. Koller, and R. Müller, Calcif. Tissue Int. **58**, 24 (1996).
[18] U. Bonse, F. Busch, O. Gunnewig, F. Beckmann, R. Pahl, G. Delling, M. Hahn, and W. Graeff, Bone Miner. **25**, 25 (1994).
[19] L. A. Feldkamp, S. A. Goldstein, A. M. Parfitt, G. Jesion, and M. Kleerekoper, J. Bone Miner. Res. **4**, 3 (1989).
[20] A. Sasov, J. Microsc. **147**, 169 (1987).
[21] B. Kanngießer, W. Malzer, A. F. Rodriguez, and I. Reiche, Spectrochim. Acta, Part B **60**, 41 (2005).
[22] G. J. Havrilla and T. C. Miller, Rev. Sci. Instrum. **76**, 062201 (2005).
[23] The measured flux in the PIN diode is equivalent to Mo $K\alpha$ (E =17.4 keV) photons.
[24] A. C. Kak and M. Slaney, *Principles of Computerized Tomographic Imaging* (IEEE, New York, 1988).
[25] C. G. Schroer, Appl. Phys. Lett. **79**, 1912 (2001).
[26] L. A. Feldkamp, L. C. Davis, and J. W. Kress, J. Opt. Soc. Am. A **1**, 612 (1984).
[27] I.-L. Lai, W. H. Schröder, J.-T. Wu, L.-L. Kuo-Huang, C. Mohl, and C.-H. Chou, Tree Physiology **27**, 1001 (2001).
[28] E. Lombi, F. J. Zhao, S. J. Dunham, and S. P. McGrath, New Phytol. **145**, 11 (2000).
[29] U. M. Cowgill and D. P. Milazzo, in *Aquatic Toxicology and Hazard Assessment*, ASTM STP Vol 12, edited by U. M. Cowgill and L. R. Williams (American Society for Testing and Materials, West Conshohocken, PA, 1989), No. 1027, pp. 379–391.
[30] The large magnification factor of 16× is achieved by placing the circuit board very close to the source (L_1=17 mm, that is, 6 mm off of the sample stage's rotation axis) using a special sample mount. In tomography mode, only magnifications up to about 12× are available in the current setup.

Downloaded 02 Jul 2007 to 141.30.244.6. Redistribution subject to AIP license or copyright, see http://rsi.aip.org/rsi/copyright.jsp